Check for updates

Synthetic engineering of neptunium oxide nanoparticles†

Ashley M. Hastings, [ID] *[a] Nic Cicchetti, [ID] [ab] Joseph R. Boro, [ID] [a] Tashi Parsons-Davis [ID] [a] and Jennifer A. Shusterman [ID] [a]

Spherical neptunium oxide nanoparticles in the 40–200 nm size range are synthesized through a homogeneous precipitation approach. These particles and their suspensions are characterized with various spectroscopic and microscopic analyses. This work bridges a gap in available size regimes for structure–property relationships in nuclear materials.

In the beginning of the atomic era, neptunium did not receive as much attention as its actinide neighbors, uranium and plutonium. Focus on neptunium manifested more in hindsight as a major activity-contributor in nuclear waste.[1,2] In the last decade, neptunium research has been reinvigorated with its central role in ^{238}Pu production for space exploration[3–5] and advanced reactor technology prospects.[6,7] In these applications, neptunium is often in its NpO_2 powder chemical form and it maintains morphological and size characteristics from the production method. The particle size and shape affect the material handling (*e.g.*, dispersibility, filterability, and packing in a consolidated form like pellets or billets). More fundamentally, particle size affects optical and electronic properties, as well as surface-based reactivity.[8] In this work, we distinguish "particles" from "grains" or "crystallites," which may refer to sub-particle units. Mastering synthetic engineering of different actinide particle size regimes and morphologies is necessary for studying structure–property relationships and tuning material properties for innovative applications.

Bulk precipitation and calcination methods result in NpO_2 with a range of particle sizes, largely >1 μm, and often lack morphological control.[9–13] For example, in the oxalate precipitation process, factors such as neptunium and oxalic/nitric acid concentrations, temperature, mixing, and order of addition all affect the Np oxalate product.[14] Conditions are selected to optimize processing scale product yield and filterability, which corresponds with larger particle size.[15,16] On the smaller end of the spectrum, Np oxide nanocrystals produced from carbonate matrix dilution[17] and thermolysis of a nitrate salt precursor[18] are reported as 2–5 nm in size. Some Np colloids (*i.e.*, an unspecified hydrated neptunium hydr(oxide) phase) have been measured as 50–60 nm in size,[19] though this is much larger than other tetravalent actinide colloids (typically 2–20 nm), and may be indicative of aggregation.[20,21] Actinide colloids are notoriously challenging to manipulate in solution and their ill-defined composition and amorphous form is not ideal for further processing or applications. Larger, sub-micron NpO_2 particles can form *via* thermolysis of an organometallic molecular precursor[22] or hydrothermal oxalate conversion.[23] However, these processes involve inert atmosphere and/or high pressure and temperature operations. We are interested in a facile synthesis of large spherical NpO_2 nanoparticles (50–100 nm) to help fill the gap of accessible NpO_2 particle sizes (Fig. 1). To minimize dispersibility hazards associated with NpO_2 particles, we focus on suspension-based manipulation and control of the
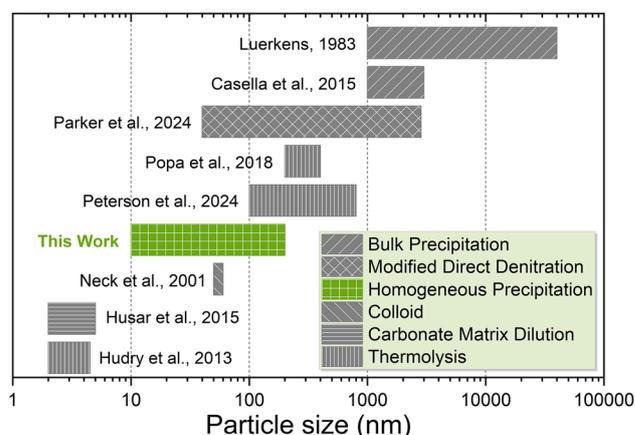
[a]Nuclear and Chemical Sciences Division, Lawrence Livermore National Laboratory, Livermore, CA 94550, USA. E-mail: hastings9@llnl.gov

[b]University of Nevada Las Vegas, Las Vegas, NV, 89154, USA

Fig. 1 Summary of reported NpO_2 size regimes *via* different synthetic routes.

particle feedstock throughout synthesis and consolidation. Particles of approximately 100 nm were targeted as a size that could both form homogeneous suspensions and be centrifuged to isolate the solid phase. Spherical particles specifically offer ideal characteristics, such as efficient packing, flow, and thermal properties.[24] Hexamethylenetetramine (HMT) has an existing role for spherical particle production in the nuclear industry for gelation processes (*e.g.*, uranium microsphere kernels for TRISO fuels).[25–28] Recently, we reported a modified homogeneous precipitation synthesis of CeO_2 particles with HMT that meets our objective criteria.[29] Herein, we share the transuranic extension to Np chemistry and subsequent materials characterization.

Neptunium oxide nanoparticles (NPs) were synthesized using a homogeneous precipitation with HMT and ammonium hydroxide in a solvent mixture of ethanol and water at room temperature. The Np was introduced as an electrochemically-reduced Np(IV) stock in dilute nitric acid (Fig. S1 and S2†). Additional synthetic details are provided in the ESI.† The HMT serves as a spherical particle templating agent and pH moderator, while the ammonium hydroxide raises the pH to induce particle nucleation through hydrolysis of Np(IV). Typically, under these conditions with Ce, the decomposition of HMT is sufficient to raise the pH without the addition of ammonium hydroxide. However, the more acidic initial solution required to prevent preemptive hydrolysis of Np(IV) interferes with the HMT decomposition process and thus ammonium hydroxide is necessary. In the synthesis, the pH was adjusted stepwise to minimize localized interfacial effects of the base introduction (Fig. 2). Nucleation of tan-colored particles is visibly evident when the pH reaches 2.0 ± 0.1. Particle flocculation is visible by pH 4.6 ± 0.1, followed by particle settling in the vial. For a reaction solution adjusted to pH 4.9 ± 0.1, the pH raised to 5.1 ± 0.1 from HMT decomposition overnight. Sampling of the supernatant after centrifugation indicates the precipitation is quantitative within experimental uncertainties above pH 4.7 ± 0.1 (further described in ESI†).

Nanoparticles were harvested, washed, and manipulated in ethanol (Fig. S3†). Dynamic light scattering (DLS) measurements on dilute Np NP samples indicate monodisperse to near-monodisperse suspensions of 40–200 nm particles (Fig. 3A). The polydispersity index (PDI) for particles synthesized at pH 4.9 was 0.10 ± 0.03(2σ). For reference, the HMT-mediated particles are more size restrained than particles synthesized at pH 7.2 with NH_4OH only (PDI = 0.21 ± 0.03) (Fig. S4†). Data collected on freshly synthesized and 11 day old particle batches indicate feedstock size distribution and dispersion consistency when aged short-term in ethanol (Fig. S5†). After proper washing (detailed in SI), dilute Np NP suspensions approach stability (*i.e.*, resistance to settling) in ethanol, demonstrated by a zeta potential value of 18.5 ± 4.3(2σ) mV (Fig. 3B). Generally, suspensions with zeta potentials of ± 30 mV are regarded as "stable".[30]

UV-vis spectra of the Np NPs in ethanol suspension are dominated by particle scattering in the near-UV range (<450 nm) (Fig. S6†). However, magnification of the 500–800 nm region reveals broad spectral features most prominent at
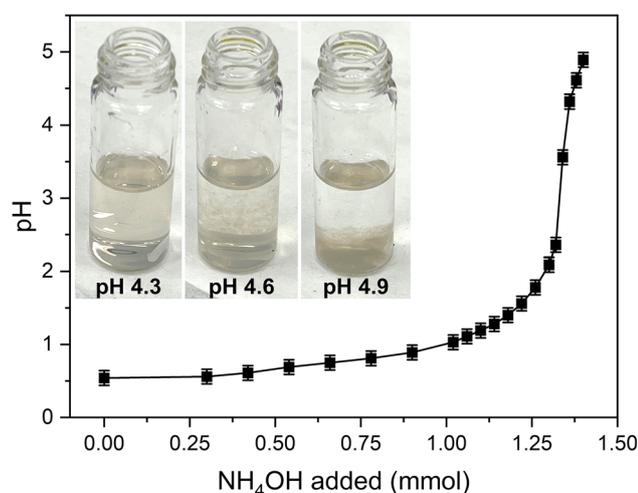

Fig. 2 Titration of the Np NP reaction solution conducted on 0.01 mmol Np (~2.4 mg Np) scale with 10 equivalents of HMT. Inset are photos at different pH points. Dispersed tan particle nucleation is evident (pH 2−4.3), followed by flocculation (pH 4.6), and settling (pH 4.9).
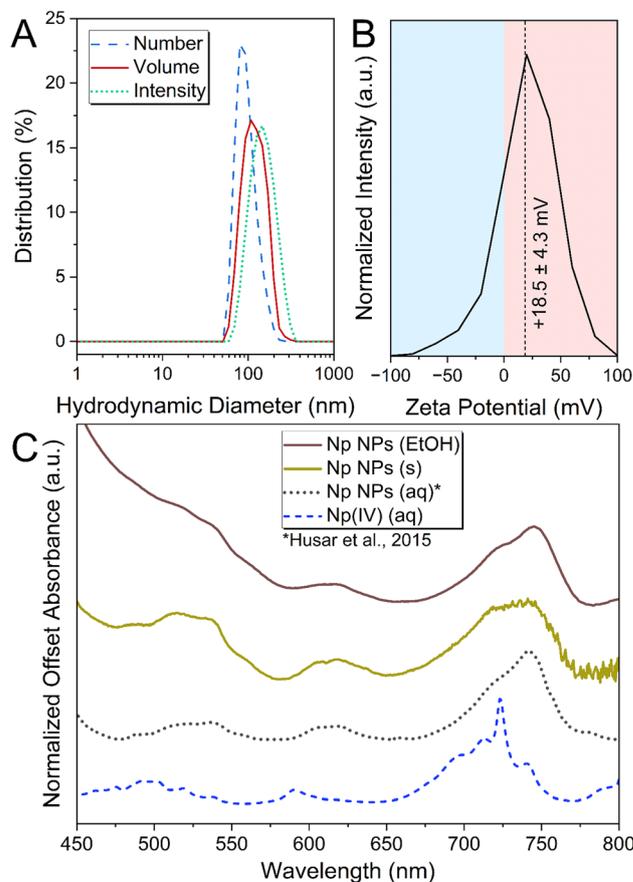

Fig. 3 Dynamic light scattering data (A) and zeta measurement (B) of Np NPs synthesized at pH 4.9. (C) UV-vis spectra of the Np NPs in ethanolic suspension and as a dried solid compared to previous report of Np nanocrystals and a reference of the Np(IV) aquo complex. Spectra were scaled for comparison.

745 nm that are distinct from the aquo Np(IV) complex (Fig. 3C). Original Np(IV) hydrolysis work describes a broad band around 700–760 nm and loss of sharp transitions.[19] These features persist in the solid state and align well with Husar *et al.*'s[17] previous report of resuspended Np nanocrystals. Conversion to Tauc plots of the solid-state spectra enabled a direct band gap estimation of $2.72 \pm 0.02(2\sigma)$ eV (Fig. S7†), which is consistent with the tan color. Our value is slightly lower than the 2.85 eV measured on a NpO_2 thin film by McCleskey *et al.*[31] Typically nanomaterials have band gaps shifted higher than that of their bulk material, though we are not aware of a true bulk band gap measurement for NpO_2.[32] As particle size decreases, the relative contributions of surface chemistry to material properties increases. Thus, the presence of adsorbed solvent, redox behavior, crystal lattice strain, or other surface-sensitive properties may have more significant contributions to optical/electronic features in nanomaterials. Our deviation may also arise from the material not undergoing any thermal treatment (*e.g.*, remaining hydrated and/or being poorly crystalline), while McCleskey *et al.*[31] high fired their NpO_2 thin film at 1000 °C. In amorphous compounds, band gaps arise from the short-range order with more diffuse energy states than crystalline compounds with long-range order.[33] Given the differences in the material synthesized here and that of McCleskey *et al.*,[31] the band gaps are in reasonable agreement.

Scanning electron microscopy on transuranic particles of this size regime is challenging to execute and approaches resolution limits of the available instrumentation. Micrographs reveal near spherical particulate of around 10–40 nm (Fig. S8†), which is smaller than the hydrodynamic diameter observed in suspension, 60–200 nm. Disparity in suspension-based *versus* solid-state particle size estimations are common and can arise from solvent effects and sampling size.[34] For example, in our preparation the DLS sample contained $30\times$ more particles than the SEM stub. Energy dispersive X-ray spectra (EDS) confirms the presence of Np in the particles and also identifies high carbon content (Fig. S9†). The absence of a nitrogen signal suggests HMT does not linger as a residue at the particle surface from its role as a templating agent. Instead, the carbon content may originate from several sources including, adsorbed ethanol, residue from the diamond polishing compound used to prepare the stub, and the common phenomenon of electron-beam-induced carbon deposition during analysis.[35]

For phase identification, the particles were analyzed by powder X-ray diffraction (PXRD), but no diffraction peaks were observed (Fig. S10†). This contrasts with the Ce NPs synthesized similarly which show poorly crystalline peaks of the CeO_2 structure, but the Ce particles are about twice the size of the Np particles.[29] The phase was further characterized by Raman spectroscopy (Fig. 4). The only band at 453 cm^{-1} is assigned to the characteristic $\Gamma_{25'}$ stretching mode, also known as the T_{2g} phonon in fluorite actinide dioxide compounds. No longitudinal optic modes are evident. We do note the susceptibility of the phase to damage under the laser (Fig. S11†); samples exposed to excess laser no longer exhibit the 453 cm^{-1} band. Sampling parameters were selected carefully to mitigate this effect, though this was challenging with the low signal from the
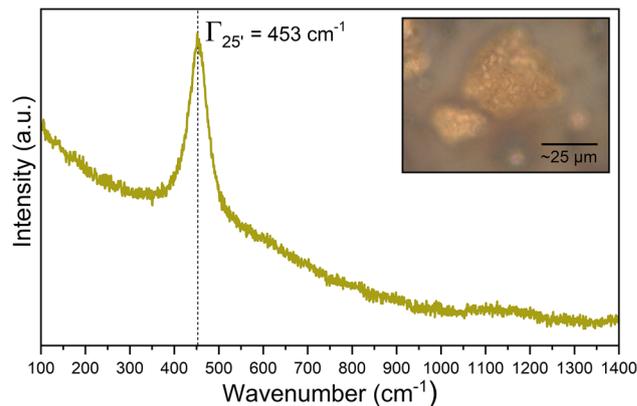

Fig. 4 Raman spectrum of Np NPs. Inset is an image taken through the 50× Raman microscope objective.

nanomaterial. It is possible that localized annealing from the laser exposure produced the NpO_2 signal and it is not intrinsic to the "as synthesized" material, especially considering the amorphous structure. Regardless, the $\Gamma_{25'}$ is 13 cm^{-1} lower than usually observed in bulk NpO_2 (466 cm^{-1}).[36] This red shift is consistent with what has previously been observed for nano-ThO_2 compared to bulk ThO_2 (3 cm^{-1}); these ThO_2 samples had undergone similar thermal treatment.[37] We suspect the larger shift in our Np sample arises from the comparison of our hydrated material to high-fired NpO_2.

We have described the size and shape-controlled synthesis of spherical neptunium oxide particles through a homogeneous precipitation approach. The synthesis has a high yield as well as monodisperse and moderately stable suspension properties, lending itself well to future use as a suspension-based particle feedstock. While the phase is not crystalline NpO_2 "as synthesized", this can be common with particles achieved by solvent-based, ambient to mild temperature methods.[28] For example, internal gelation processes produce hydrous metal oxide microspheres.[28] Our approach, which delves into the nanoscale, appears to have a similar result. We have demonstrated the ability to manipulate the nanoparticles and avoid aggregation, which is essential to their functionality; subsequent formal conversion to crystalline NpO_2 through heat treatment is possible. Furthermore, feedstocks commonly undergo thermal processing once consolidated to dry the product, remove any organic content, and densify the form (*e.g.*, sintering of pressed pellets). Accessibility to particles of these characteristics for nuclear materials has implications that span fundamental to applied actinide science.

Data availability

The data supporting this article have been included as part of the ESI.†

Author contributions

A. M. H: conceptualization, investigation, writing – original draft; N. C.: investigation; J. R. B.: formal analysis and

resources; T. P.-D.: supervision; J. A. S.: conceptualization, supervision, writing – review & editing, funding acquisition.

Conflicts of interest

There are no conflicts to declare.

Acknowledgements

Notes and references

1 B. L. Cohen, *Health Phys.*, 1982, **42**, 133–143.
2 P. Thakur and G. P. Mulholland, *Appl. Radiat. Isot.*, 2012, **70**, 1747–1778.
3 L. R. Sadergaski, K. K. Patton, G. K. Toney and D. W. DePaoli, *Measuring Neptunium Concentration Using Optical Spectrometry for the Plutonium-238 Supply Program*, Oak Ridge National Laboratory, Oak Ridge, TN, 2021.
4 K. M. Peruski, *Front. Nucl. Eng.*, 2022, **1**, 1–7.
5 K. M. Peruski, C. J. Parker and S. K. Cary, *J. Nucl. Mater.*, 2023, **587**, 154704.
6 V. A. Apse, A. N. Shmelev, G. G. Kulikov and E. G. Kulikov, *Phys. Atom. Nuclei*, 2018, **81**, 1531–1535.
7 E. P. Shabalin, V. L. Aksenov, G. G. Komyshev and A. D. Rogov, *At. Energy*, 2018, **124**, 364–370.
8 R. M. Pallares and R. J. Abergel, *Nanoscale*, 2020, **12**, 1339–1348.
9 A. L. Tamasi, L. J. Cash, C. Eley, R. B. Porter, D. L. Pugmire, A. R. Ross, C. E. Ruggiero, L. Tandon, G. L. Wagner, J. R. Walensky, A. D. Wall and M. P. Wilkerson, *J. Radioanal. Nucl. Chem.*, 2016, **307**, 1611–1619.
10 J. L. Doyle, D. Schwartz and L. Tandon, *MRS Adv.*, 2016, **1**, 2999–3005.
11 K. M. Peruski, K. C. Koehler and B. A. Powell, *Environ. Sci.: Nano*, 2020, **7**, 2293–2301.
12 A. M. Casella, R. D. Scheele and B. K. McNamara, *AIP Adv.*, 2015, **5**, 127230.
13 C. J. Parker, K. M. Peruski and S. K. Cary, *Microsc. Microanal.*, 2025, **31**, 1–8.
14 D. W. Luerkens, *Two-Stage Precipitation of Neptunium (IV) Oxalate*, Savannah River Laboratory, Aiken, SC, 1983.
15 J. A. Porter, *Precipitation of Neptunium Oxalate and Calcination to Neptunium Oxide*, Savannah River Laboratory, Aiken, SC, 1961.
16 J. A. Porter, *Ind. Eng. Chem. Proc. Des. Dev.*, 1964, **3**, 289–292.

17 R. Husar, R. Hübner, C. Hennig, P. M. Martin, M. Chollet, S. Weiss, T. Stumpf, H. Zänker and A. Ikeda-Ohno, *Chem. Commun.*, 2015, **51**, 1301–1304.
18 D. Hudry, C. Apostolidis, O. Walter, T. Gouder, A. Janssen, E. Courtois, C. Kübel and D. Meyer, *RSC Adv.*, 2013, **3**, 18271–18274.
19 V. Neck, J. I. Kim, B. S. Seidel, C. M. Marquardt, K. Dardenne, M. P. Jensen and W. Hauser, *Radiochim. Acta*, 2001, **89**, 439–446.
20 T. Bundschuh, R. Knopp, R. Müller, J. I. Kim, V. Neck and T. Fanghänel, *Radiochim. Acta*, 2000, **88**, 625–632.
21 A. B. Kersting, *Inorg. Chem.*, 2013, **52**, 3533–3546.
22 A. Peterson, S. N. Kelly, T. Arino, S. O. Gunther, E. T. Ouellette, J. N. Wacker, J. J. Woods, S. J. Teat, W. W. Lukens, J. Arnold, R. J. Abergel and S. G. Minasian, *Inorg. Chem.*, 2024, **63**, 18417–18428.
23 K. Popa, O. Walter, O. D. Blanco, A. Guiot, D. Bouëxière, J.-Y. Colle, L. Martel, M. Naji and D. Manara, *CrystEngComm*, 2018, **20**, 4614–4622.
24 M. Zach, D. Brashear, J. Duran, Ł. Żrodowski, B. Kalicki, T. Choma, M. Sołowiow and S. Adler, *EPJ Web Conf.*, 2023, **285**, 03002.
25 R. D. Hunt and J. L. Collins, *Radiochim. Acta*, 2004, **92**, 909–915.
26 R. D. Hunt, J. L. Collins, M. H. Lloyd and S. C. Finkeldei, *J. Nucl. Mater.*, 2019, **515**, 107–110.
27 J. A. Phillips, S. G. Nagley and E. L. Shaber, *Nucl. Eng. Des.*, 2012, **251**, 261–281.
28 J. A. Katalenich and B. B. Kitchen, *J. Sol-Gel Sci. Technol.*, 2021, **98**, 288–299.
29 A. M. Hastings, S. Herrera, S. Harris, T. Parsons-Davis, A. J. Pascall and J. A. Shusterman, *Dalton Trans.*, 2024, **53**, 7376–7383.
30 R. Xu, C. Wu and H. Xu, *Carbon*, 2007, **45**, 2806–2809.
31 T. M. McCleskey, E. Bauer, Q. Jia, A. K. Burrell, B. L. Scott, S. D. Conradson, A. Mueller, L. Roy, X. Wen, G. E. Scuseria and R. L. Martin, *J. Appl. Phys.*, 2013, **113**, 013515.
32 Y. Dieckmann, H. Cölfen, H. Hofmann and A. Petri-Fink, *Anal. Chem.*, 2009, **81**, 3889–3895.
33 N. Sato, in *Electrochemistry at Metal and Semiconductor Electrodes*, ed. N. Sato, Elsevier Science, Amsterdam, 1998, pp. 15–59.
34 M. F. McLaughlin, J. Woodward, R. A. Boll, J. S. Wall, A. J. Rondinone, S. J. Kennel, S. Mirzadeh and J. D. Robertson, *PLoS One*, 2013, **8**, e54531.
35 D. Lau, A. E. Hughes, T. H. Muster, T. J. Davis and A. M. Glenn, *Microsc. Microanal.*, 2010, **16**, 13–20.
36 M. Naji, N. Magnani, J.-Y. Colle, O. Beneš, S. Stohr, R. Caciuffo, R. J. M. Konings and D. Manara, *J. Phys. Chem. C*, 2016, **120**, 4799–4805.
37 S. Dash, A. Singh, P. K. Ajikumar, H. Subramanian, M. Rajalakshmi, A. K. Tyagi, A. K. Arora, S. V. Narasimhan and B. Raj, *J. Nucl. Mater.*, 2002, **303**, 156–168.